Supplement of Atmos. Chem. Phys., 16, 7411–7433, 2016
http://www.atmos-chem-phys.net/16/7411/2016/
doi:10.5194/acp-16-7411-2016-supplement

Atmospheric Chemistry and Physics Open Access EGU

Supplement of

Real-time measurements of secondary organic aerosol formation and aging from ambient air in an oxidation flow reactor in the Los Angeles area

Amber M. Ortega et al.

Correspondence to: Jose L. Jimenez (jose.jimenez@colorado.edu)

1 Quantification of AMS Reactor Data

All aspects of quantification of AMS data are the same as described by Hayes et al. (2013). Here we describe only those aspects where additional analysis or corrections are needed specifically for the reactor output data.

1.1 AMS Collection Efficiency

Quantification of AMS concentration data requires a correction for particle bounce at the vaporizer, referred to as the collection efficiency (CE; Canagaratna et al., 2007). The composition-dependent CE formulation of Middlebrook et al. (2012) was used by Hayes et al. (2013) to estimate CE for the ambient data, leading to good intercomparisons with multiple collocated instruments as documented by that study. The same methodology has also been applied to reactor output measurements.

Although the focus of this paper is OA formation and aging, a brief summary of the observed evolution of the inorganic species: (a) Sulfate formation proceeds as expected from the OH + SO_2 reaction. A quantitative analysis of sulfate formation is shown in Palm et al. (2016), which reports results from a similar experiment from our group, but in a forest environment. That analysis provides evidence that the corrections for losses of low volatility species developed in that work are appropriate. (b) Nitrate formation is more complex since OH + NO_2 is a fast reaction, but HNO_3 is semivolatile and the formation of NH_4NO_3 also depends on the availability of NH_3(g). (c) The aerosols in the output of the flow reactor during CalNex are neutralized, similarly to the ambient aerosols (Hayes et al., 2013).

Fig. S2a shows the time series of reactor and ambient aerosol concentrations and estimated CE. Ambient CE periodically rises above 0.5 due to larger fractions of ammonium nitrate aerosol, which leads to reduced particle bounce (Middlebrook et al., 2012). The reactor typically formed additional ammonium sulfate and ammonium nitrate beyond ambient concentrations at the same time as ambient levels peak for those compounds, thus the reactor CE profile has a very similar temporal structure to ambient. However, Fig. S2b shows that the estimated CE increases at the highest reactor OH_{exp}, due to additional ammonium nitrate formation in the reactor with increased photochemical age.

Highly acidic particles, as indicated by the ammonium balance, can also lead to increased CE in the AMS (Middlebrook et al., 2012). The ammonium balance method compares the measured ammonium to that required to fully neutralize observed sulfate, nitrate, and chloride (Zhang et al., 2007), as shown in Fig. S3. Ambient and reactor results have near identical slopes that are indistinguishable from the one-to-one line within the uncertainties of the measurements, signifying full neutralization for both. Furthermore, this comparison indicates that the reactor is producing similar inorganic composition to that observed in the atmosphere as nitric acid and sulfuric acid gases are formed in the reactor and fully neutralized by ammonium forming ammonium nitrate and ammonium sulfate. Thus no correction of CE due to the presence of highly acidic particles are needed in this study.

Comparison of AMS and SMPS measurements for ambient and reactor data, shows that ambient data falls along a one-to-one line, indicating both instruments are measuring the same amount of mass within the uncertainties (Fig. S4a). Reactor output data has a slightly higher slope of 1.14, i.e. the AMS measures ~14% higher mass than the SMPS from the reactor and also shows a cluster of points where SMPS>AMS due to periods where substantial mass is formed at small particle

sizes (see below). Both slopes are within the combined uncertainties of the two measurements. Fig. S4b shows the relative increase in aerosol concentration in the reactor (i.e. ratio of reactor to ambient concentrations) for the SMPS vs. AMS which also compare well, on average (slope = 1.05), but with considerable scatter, most of which is likely due to additional measurement noise introduced from ratioing multiple short measurements. Evaporation of freshly formed NH_4NO_3 in the longer residence times in the SMPS (compared to the faster AMS analysis) where the sheath flow may have reduced NH_3 and HNO_3 gas concentrations, has been observed with this experimental setup, and may be a cause of the slightly larger slope for reactor output conditions. A small underestimation of AMS CE for the reactor conditions could also result in this observation.

It is also possible that the AMS relative ionization efficiency (RIE) of organic species is lower for more oxidized species (Jimenez et al., 2003; D. Murphy, pers. Comm. 2015), although no clear evidence has been reported for ambient data (e.g. Docherty et al., 2011). If that effect played a dominant role here, we would expect the reactor slopes to be lower, rather than slightly higher than 1. Thus we conclude that any RIE changes are small and cannot be separated from other effects such as small changes in CE, nitrate evaporation in the SMPS, or differences in particle transmission (next section).

1.2 Accounting for Particle Mass below the AMS Lens Transmission

As the reactor exposed ambient air to high levels of OH and O_3, new particle formation and growth was sometimes observed. To fully account for the mass of all particles formed in the reactor, it is necessary to quantify the mass of small particles below the AMS lens transmission size (Zhang et al., 2004). SMPS data was used to estimate the total mass concentration below the AMS size cut. First, particle transmission from plumbing line losses was corrected using the Particle Loss

Calculator (von der Weiden et al., 2009) for this experimental plumbing and flowrate configuration for both reactor and ambient SMPS data, with transmission curves as shown in Fig. S5. Second, the measured SMPS mass that is below the AMS transmission curve was estimated using a published AMS lens transmission parameterization (Knote et al., 2011) multiplying the SMPS size-dependent mass by the size-dependent AMS lens fractional loss (1-transmission). Figure S6a shows a time series of estimated reactor and ambient mass missed by the AMS due to transmission losses. Since corrections needed to account for the contribution of these small sizes to total mass is small for ambient data (on average 1.7%), Hayes et al. (2013) did not apply a correction to AMS ambient data. Fig. S6b shows the estimated fraction of the reactor output mass that is below the AMS lens transmission size vs. total photochemical age in days (at OH = 1.5×10^6 molec. cm^{-3}). An average of 6.2% of the total reactor output mass is estimated to be below the AMS lens transmission, with no dependence on photochemical age except possibly at the highest values (>20 days of age).

We note that the AMS measurements from the reactor may be biased ~6% low, on average, and sometimes as much as 20%. This non-measured mass likely has a large OA fraction (see Fig. S8). Thus, reactor-reported mass enhancement above ambient may be underestimated by these amounts. Given the 6.2% AMS underestimation from particle transmission of small sizes in the reactor, and the apparent 14% overestimation in the AMS vs SMPS comparison, but overall good agreement in the relative enhancement of total aerosol between both instruments, we have not corrected for these differences as the net correction would be small and within the uncertainties of the measurement, while the correction process would introduce additional noise.

Supplementary Captions

Figure S1: Results of computerized fluid dynamics (CFD) simulations comparing two OFR configurations. **(a)** Tube inlet, similar to Lambe et al. (2011); **(b)** Large open face inlet (11.9 cm diameter) as used in this field study. Colors are contours of positive horizontal velocity. White regions involve horizontal velocities, i.e. recirculation regions. The extensive recirculation regions of case (a) are almost completely removed in case (b), resulting in a narrower residence time distribution. Simulations were conducted using the FLUENT software, using cylindrical symmetry, with air at 1 atm and 293 K.

Figure S2: (a) Estimated AMS collection efficiency (CE) and corresponding AMS mass concentration time series for ambient and reactor data (after applying CE correction). **(b)** Estimated CE vs. OH exposure (OH_{exp}) in the reactor for all reactor measurements and averages for 7% quantiles.

Figure S3: Measured vs. predicted ammonium assuming full neutralization ("Ammonium balance") for ambient and reactor data. Linear orthogonal distance regression fit lines, slope and R^2 for each are also shown.

Figure S4: (a) Scatter plot of AMS mass vs. mass estimated from SMPS measurements for ambient and reactor data, with linear orthogonal distance regression fit slope and R^2 for each. A one-to-one line and +/-15% region is shown for reference. **(b)** Relative enhancement ratio from AMS and SMPS data with raw data, 20-minute averaged smooth data, linear orthogonal distance regression, line, fit slope and R^2 for each.

Figure S5: Estimated particle transmission of inlet plumbing vs. particle diameter for reactor and ambient sampling lines for both AMS and SMPS measurements, calculated using the particle loss calculator of von der Weiden et al. (2009).

Figure S6: (a) Time series of SMPS mass measured below the AMS lens transmission size for ambient and reactor measurements. **(b)** Percent of estimated mass not measured by AMS, due to on particle losses in sampling lines and the AMS lens transmission at small sizes, for the reactor vs. total photochemical age in days (at OH = 1.5×10^6 molec. cm^{-3}), where all data is colored by ΔOA mass with average 5% quantiles and standard error bars.

Figure S7: Modeled fate of low volatility organic gases (LVOCs) formed in the reactor vs. OH_{exp} including wall loss, reaction with OH, condensation on aerosol, and exiting the reactor, with a fit for the fraction condensing on aerosols in the reactor.

Figure S8: AMS mass size distribution (vs. vacuum aerodynamic diameter, d_{va}) for reactor and ambient OA, averaged from 20:00 on 2 June 2010 – 00:20 on 9 June 2010 for average nighttime ambient and reactor with no internal OH_{exp} (dark reactor), and for ~3.7 days and ~23.5 days aging.

Figure S9: Times series of benzene, 1,3,5-trimethylbenzene, and toluene on top panel. Time series of ambient OOA, reactor OA mass enhancement, maximum reactor mass enhancement, and O_x on bottom panel.

Figure S10: Ratio of organic aerosol to excess carbon monoxide (above background) vs. total photochemical age in days (at OH = 1.5×10^6 molec. cm^{-3}) for **(a)** the same data as Fig. 9, showing all data used to produce averages for quantiles of ambient and reactor vapor-loss corrected data. Also shown are the expected decays of benzene, toluene, and 1,3,5-trimethylbenzene in the reactor vs. total photochemical age in days (at OH = 1.5×10^6 molec. cm^{-3}), using reaction rates from Atkinson et al. (2006). **(b)** The same data as Fig. 9, showing reactor vapor loss-corrected data, but where excess CO is decreased by reaction with OH in the reactor, including means for 12% quantiles. Results from field studies in the northeastern US and Mexico City are shown for comparison to previous observations (DeCarlo et al., 2010). A fit to the data when CO is assumed to react with OH is shown.

Figure S11: The ratio of the gain of oxygen of OA observed in the reactor (ΔOxygen in OA = $O_{atoms,\ reactor} - O_{atoms,\ ambient}$) to the total number of OH collisions with OA in the reactor vs. total photochemical age. The estimated number of OH collisions is calculated based on the methodology outlined in appendix A of DeCarlo et al. (2008).

Figure S12: Top panel: Mass fraction remaining (MFR) for OA vs. thermal denuder temperature for this CalNex-LA dataset, using the methods described in Huffman et al. (2008; 2009). Bottom panel: estimated volatility distribution of particle- and gas-phase species, calculated from the thermal denuder profile using the method of Faulhaber et al. (2009), on bottom panel.

References

Atkinson, R., Baulch, D. L., Cox, R. A., Crowley, J. N., Hampson, R. F., Hynes, R. G., Jenkin, M. E., Rossi, M. J., Troe, J., and Subcommittee, I.: Evaluated kinetic and photochemical data for atmospheric chemistry: Volume II: gas phase reactions of organic species, Atmos. Chem. Phys., 6, 3625-4055, 10.5194/acp-6-3625-2006, 2006.

Canagaratna, M. R., Jayne, J. T., Jimenez, J. L., Allan, J. D., Alfarra, M. R., Zhang, Q., Onasch, T. B., Drewnick, F., Coe, H., Middlebrook, A., Delia, A., Williams, L. R., Trimborn, A. M., Northway, M. J., DeCarlo, P. F., Kolb, C. E., Davidovits, P., and Worsnop, D. R.: Chemical and microphysical characterization of ambient aerosols with the aerodyne aerosol mass spectrometer, Mass Spectrom Rev, 26, 185-222, Doi 10.1002/Mas.20115, 2007.

DeCarlo, P. F., Dunlea, E. J., Kimmel, J. R., Aiken, A. C., Sueper, D., Crounse, J., Wennberg, P. O., Emmons, L., Shinozuka, Y., Clarke, A., Zhou, J., Tomlinson, J., Collins, D. R., Knapp, D., Weinheimer, A. J., Montzka, D. D.,

158 Campos, T., and Jimenez, J. L.: Fast airborne aerosol size and chemistry measurements above Mexico City and Central
159 Mexico during the MILAGRO campaign, Atmos. Chem. Phys., 8, 4027-4048, 10.5194/acp-8-4027-2008, 2008.

160 DeCarlo, P. F., Ulbrich, I. M., Crounse, J., de Foy, B., Dunlea, E. J., Aiken, A. C., Knapp, D., Weinheimer, A. J.,
161 Campos, T., Wennberg, P. O., and Jimenez, J. L.: Investigation of the sources and processing of organic aerosol over
162 the Central Mexican Plateau from aircraft measurements during MILAGRO, Atmos. Chem. Phys., 10, 5257-5280,
163 10.5194/acp-10-5257-2010, 2010.

164 Docherty, K. S., Aiken, A. C., Huffman, J. A., Ulbrich, I. M., DeCarlo, P. F., Sueper, D., Worsnop, D. R., Snyder, D.
165 C., Peltier, R. E., Weber, R. J., Grover, B. D., Eatough, D. J., Williams, B. J., Goldstein, A. H., Ziemann, P. J., and
166 Jimenez, J. L.: The 2005 Study of Organic Aerosols at Riverside (SOAR-1): instrumental intercomparisons and fine
167 particle composition, Atmos. Chem. Phys., 11, 12387-12420, 10.5194/acp-11-12387-2011, 2011.

168 Faulhaber, A. E., Thomas, B. M., Jimenez, J. L., Jayne, J. T., Worsnop, D. R., and Ziemann, P. J.: Characterization of
169 a thermodenuder-particle beam mass spectrometer system for the study of organic aerosol volatility and composition,
170 Atmos. Meas. Tech., 2, 15-31, 10.5194/amt-2-15-2009, 2009.

171 Hayes, P. L., Ortega, A. M., Cubison, M. J., Froyd, K. D., Zhao, Y., Cliff, S. S., Hu, W. W., Toohey, D. W., Flynn, J.
172 H., Lefer, B. L., Grossberg, N., Alvarez, S., Rappenglück, B., Taylor, J. W., Allan, J. D., Holloway, J. S., Gilman, J.
173 B., Kuster, W. C., de Gouw, J. A., Massoli, P., Zhang, X., Liu, J., Weber, R. J., Corrigan, A. L., Russell, L. M.,
174 Isaacman, G., Worton, D. R., Kreisberg, N. M., Goldstein, A. H., Thalman, R., Waxman, E. M., Volkamer, R., Lin,
175 Y. H., Surratt, J. D., Kleindienst, T. E., Offenberg, J. H., Dusanter, S., Griffith, S., Stevens, P. S., Brioude, J.,
176 Angevine, W. M., and Jimenez, J. L.: Organic aerosol composition and sources in Pasadena, California, during the
177 2010 CalNex campaign, Journal of Geophysical Research: Atmospheres, 118, 9233-9257, 10.1002/jgrd.50530, 2013.

178 Huffman, J. A., Ziemann, P. J., Jayne, J. T., Worsnop, D. R., and Jimenez, J. L.: Development and Characterization
179 of a Fast-Stepping/Scanning Thermodenuder for Chemically-Resolved Aerosol Volatility Measurements, Aerosol
180 Science and Technology, 42, 395-407, 10.1080/02786820802104981, 2008.

181 Huffman, J. A., Docherty, K. S., Aiken, A. C., Cubison, M. J., Ulbrich, I. M., DeCarlo, P. F., Sueper, D., Jayne, J. T.,
182 Worsnop, D. R., Ziemann, P. J., and Jimenez, J. L.: Chemically-resolved aerosol volatility measurements from two
183 megacity field studies, Atmos. Chem. Phys., 9, 7161-7182, 10.5194/acp-9-7161-2009, 2009.

184 Jimenez, J. L., Jayne, J. T., Shi, Q., Kolb, C. E., Worsnop, D. R., Yourshaw, I., Seinfeld, J. H., Flagan, R. C., Zhang,
185 X. F., Smith, K. A., Morris, J. W., and Davidovits, P.: Ambient aerosol sampling using the Aerodyne Aerosol Mass
186 Spectrometer, J Geophys Res-Atmos, 108, 2003.

187 Knote, C., Brunner, D., Vogel, H., Allan, J., Asmi, A., Äijälä, M., Carbone, S., van der Gon, H. D., Jimenez, J. L.,
188 Kiendler-Scharr, A., Mohr, C., Poulain, L., Prévôt, A. S. H., Swietlicki, E., and Vogel, B.: Towards an online-coupled
189 chemistry-climate model: evaluation of trace gases and aerosols in COSMO-ART, Geosci. Model Dev., 4, 1077-1102,
190 10.5194/gmd-4-1077-2011, 2011.

191 Lambe, A. T., Onasch, T. B., Massoli, P., Croasdale, D. R., Wright, J. P., Ahern, A. T., Williams, L. R., Worsnop, D.
192 R., Brune, W. H., and Davidovits, P.: Laboratory studies of the chemical composition and cloud condensation nuclei
193 (CCN) activity of secondary organic aerosol (SOA) and oxidized primary organic aerosol (OPOA), Atmos Chem
194 Phys, 11, 8913-8928, DOI 10.5194/acp-11-8913-2011, 2011.

195 Middlebrook, A. M., Bahreini, R., Jimenez, J. L., and Canagaratna, M. R.: Evaluation of Composition-Dependent
196 Collection Efficiencies for the Aerodyne Aerosol Mass Spectrometer using Field Data, Aerosol Sci Tech, 46, 258-
197 271, 2012.

198 Palm, B. B., Campuzano-Jost, P., Ortega, A. M., Day, D. A., Kaser, L., Jud, W., Karl, T., Hansel, A., Hunter, J. F.,
199 Cross, E. S., Kroll, J. H., Peng, Z., Brune, W. H., and Jimenez, J. L.: In situ secondary organic aerosol formation from
200 ambient pine forest air using an oxidation flow reactor, Atmos. Chem. Phys., 16, 2943-2970, 10.5194/acp-16-2943-
201 2016, 2016.

202 von der Weiden, S. L., Drewnick, F., and Borrmann, S.: Particle Loss Calculator – a new software tool for the
203 assessment of the performance of aerosol inlet systems, Atmos. Meas. Tech. Discuss., 2, 1099-1141, 10.5194/amtd-
204 2-1099-2009, 2009.

205 Zhang, Q., Jimenez, J. L., Canagaratna, M. R., Allan, J. D., Coe, H., Ulbrich, I., Alfarra, M. R., Takami, A.,
206 Middlebrook, A. M., Sun, Y. L., Dzepina, K., Dunlea, E., Docherty, K., DeCarlo, P. F., Salcedo, D., Onasch, T., Jayne,
207 J. T., Miyoshi, T., Shimono, A., Hatakeyama, S., Takegawa, N., Kondo, Y., Schneider, J., Drewnick, F., Borrmann,
208 S., Weimer, S., Demerjian, K., Williams, P., Bower, K., Bahreini, R., Cottrell, L., Griffin, R. J., Rautiainen, J., Sun,
209 J. Y., Zhang, Y. M., and Worsnop, D. R.: Ubiquity and dominance of oxygenated species in organic aerosols in
210 anthropogenically-influenced Northern Hemisphere midlatitudes, Geophys. Res. Lett., 34, L13801,
211 10.1029/2007gl029979, 2007.

212 Zhang, X. F., Smith, K. A., Worsnop, D. R., Jimenez, J. L., Jayne, J. T., Kolb, C. E., Morris, J., and Davidovits, P.:
213 Numerical characterization of particle beam collimation: Part II - Integrated aerodynamic-lens-nozzle system, Aerosol
214 Science and Technology, 38, 619-638, 10.1080/02786820490479833, 2004.

215

216

Figure S1.

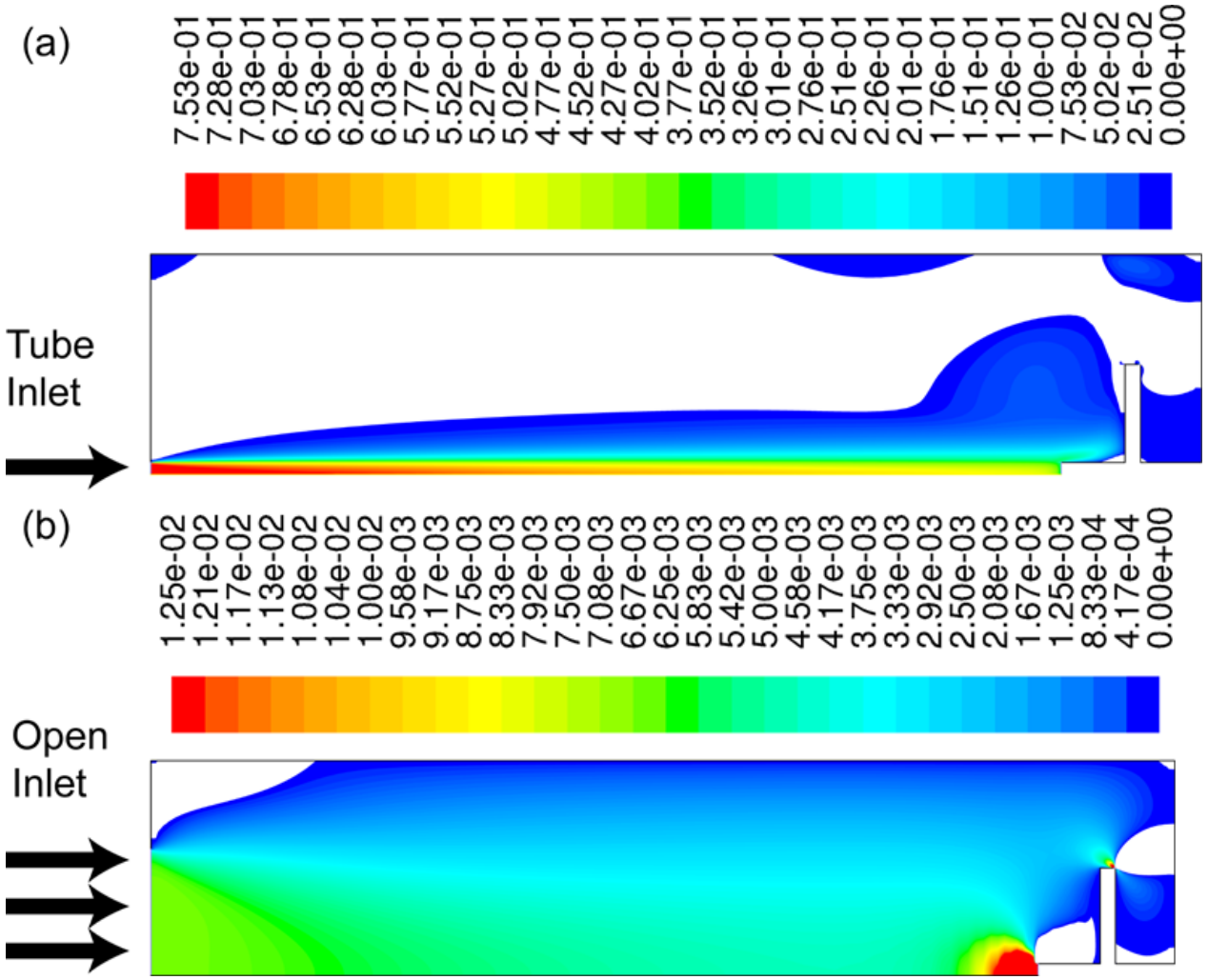
(a)
7.53e-01
7.28e-01
7.03e-01
6.78e-01
6.53e-01
6.28e-01
6.03e-01
5.77e-01
5.52e-01
5.27e-01
5.02e-01
4.77e-01
4.52e-01
4.27e-01
4.02e-01
3.77e-01
3.52e-01
3.26e-01
3.01e-01
2.76e-01
2.51e-01
2.26e-01
2.01e-01
1.76e-01
1.51e-01
1.26e-01
1.00e-01
7.53e-02
5.02e-02
2.51e-02
0.00e+00
Tube
Inlet
(b)
1.25e-02
1.21e-02
1.17e-02
1.13e-02
1.08e-02
1.04e-02
1.00e-02
9.58e-03
9.17e-03
8.75e-03
8.33e-03
7.92e-03
7.50e-03
7.08e-03
6.67e-03
6.25e-03
5.83e-03
5.42e-03
5.00e-03
4.58e-03
4.17e-03
3.75e-03
3.33e-03
2.92e-03
2.50e-03
2.08e-03
1.67e-03
1.25e-03
8.33e-04
4.17e-04
0.00e+00
Open
Inlet

Figure S2.

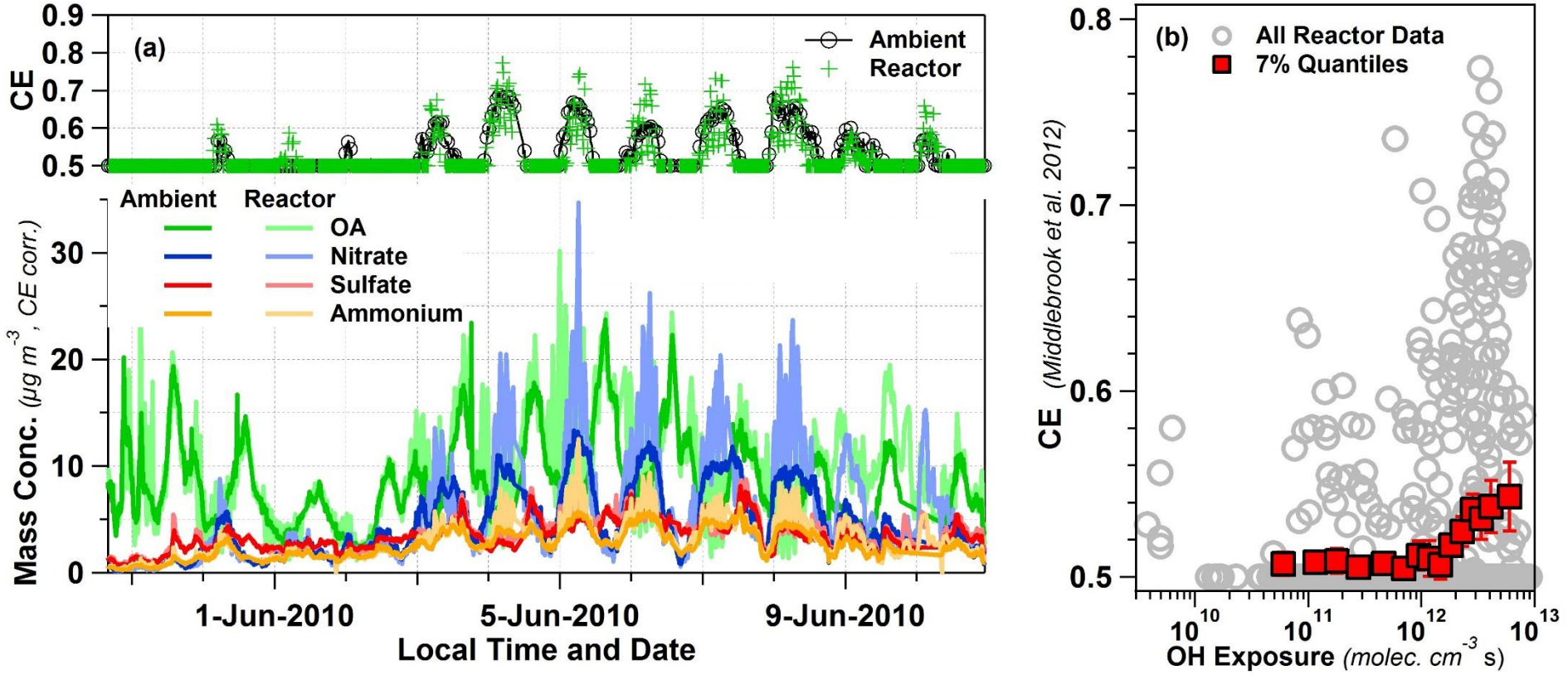
(a)
Ambient
Reactor
CE
0.9
0.8
0.7
0.6
0.5
Ambient
Reactor
OA
Nitrate
Sulfate
Ammonium
Mass Conc. (μg m-3, CE corr.)
30
20
10
0
1-Jun-2010
5-Jun-2010
9-Jun-2010
Local Time and Date
(b)
All Reactor Data
7% Quantiles
CE (Middlebrook et al. 2012)
0.8
0.7
0.6
0.5
10^10
10^11
10^12
10^13
OH Exposure (molec. cm-3 s)

Figure S3.

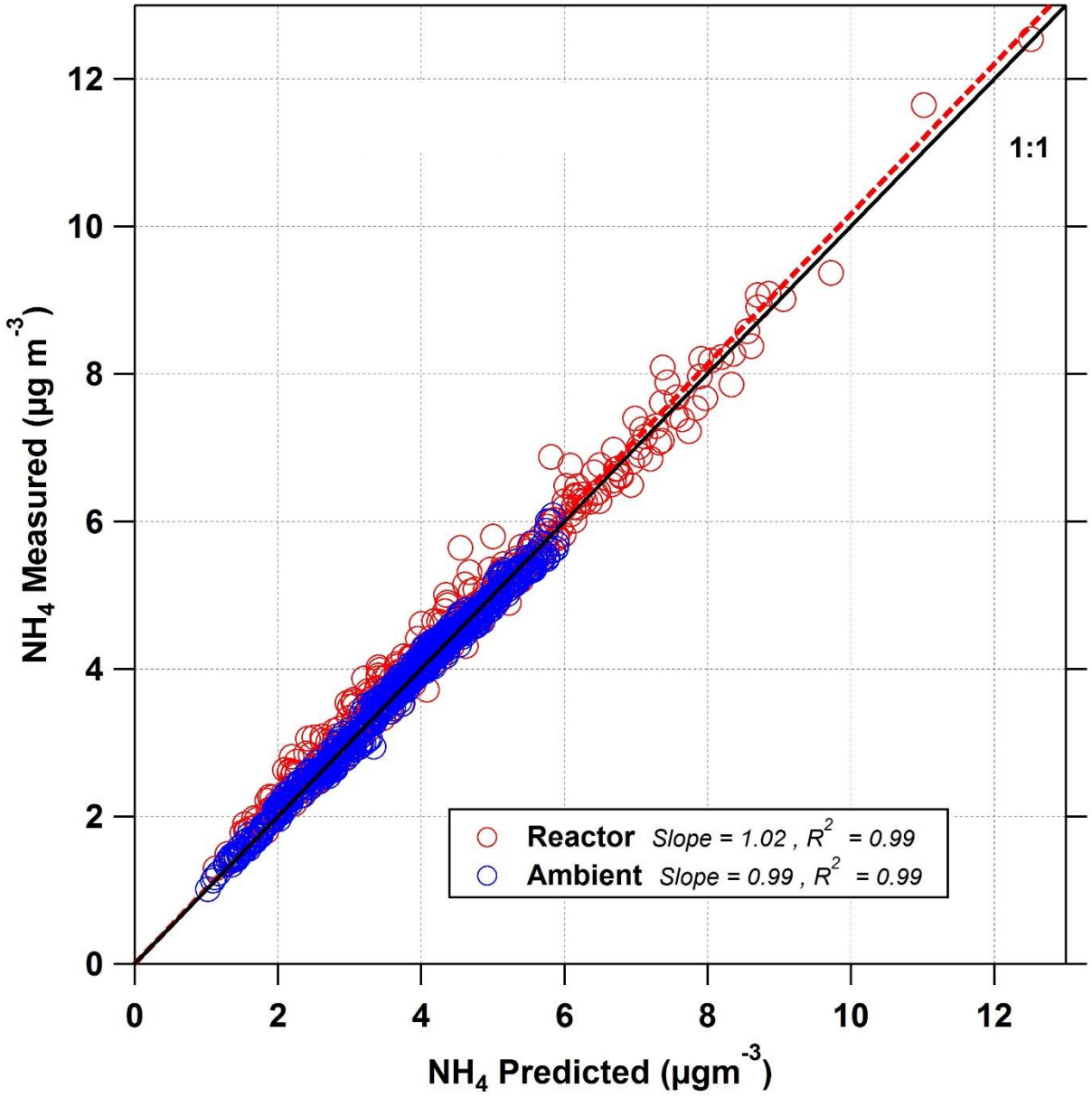
12
10
8
6
4
2
0
0
2
4
6
8
10
12
1:1
NH4 Measured (µg m-3)
NH4 Predicted (µgm-3)
Reactor Slope = 1.02 , R2 = 0.99
Ambient Slope = 0.99 , R2 = 0.99

Figure S4.

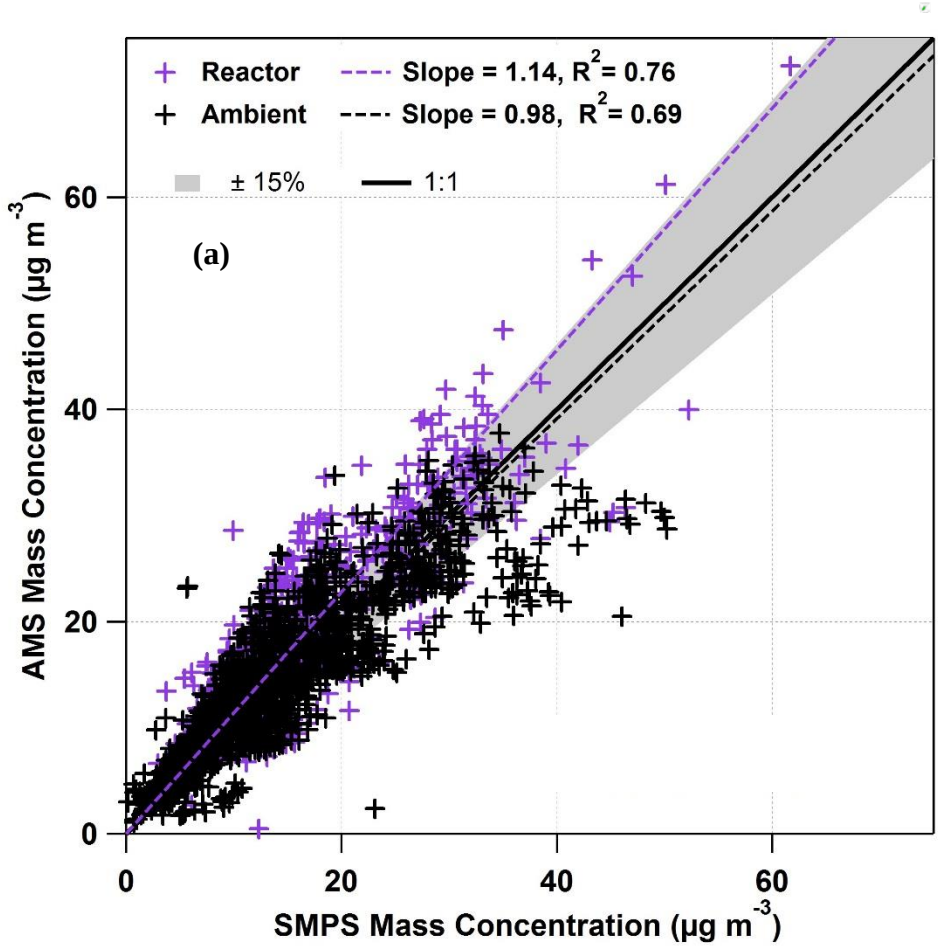
Reactor
Slope = 1.14, R2 = 0.76
Ambient
Slope = 0.98, R2 = 0.69
± 15%
1:1
(a)
AMS Mass Concentration (µg m-3)
SMPS Mass Concentration (µg m-3)
0
20
40
60

(b)

Figure S5.

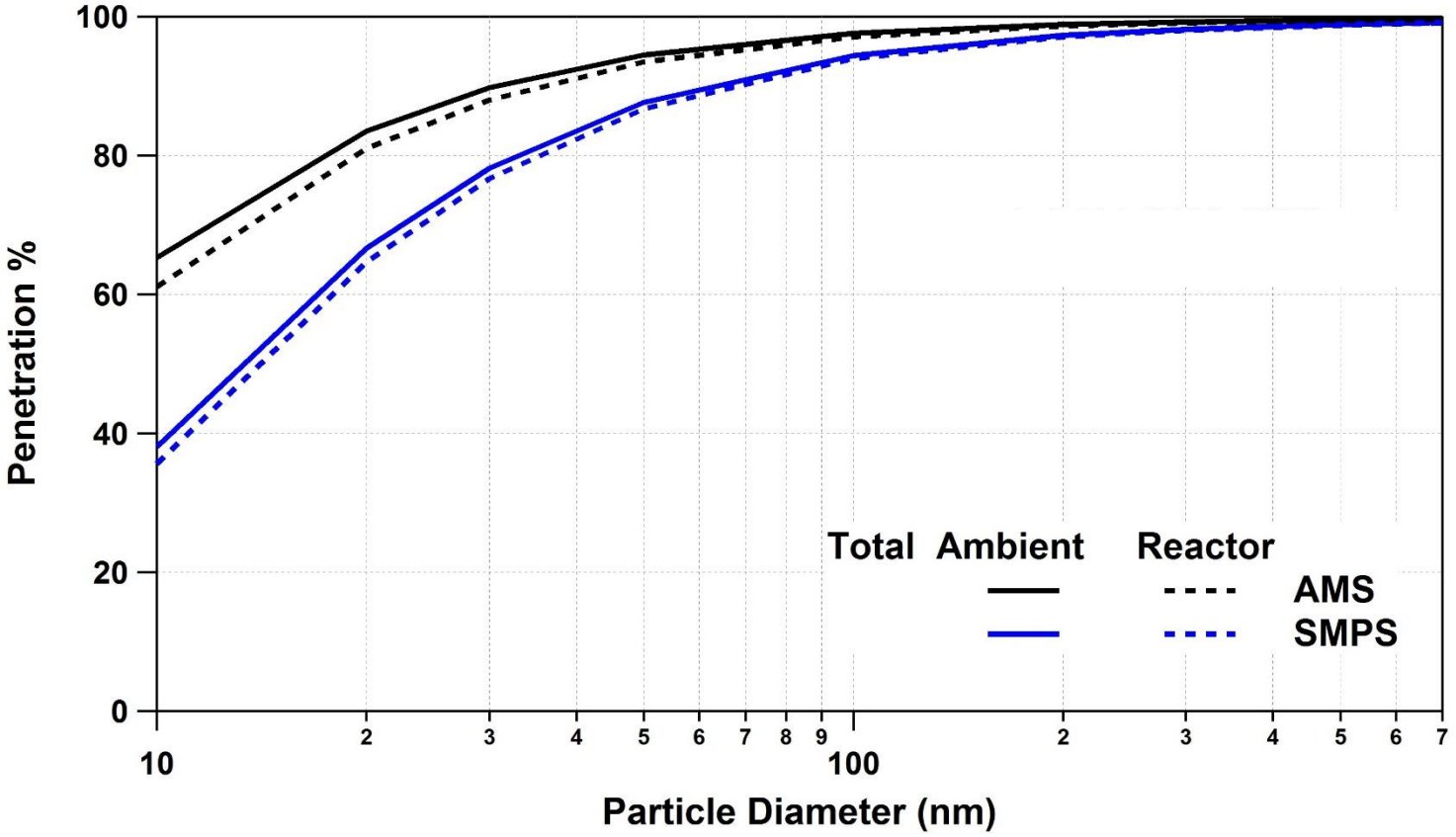
Penetration %
100
80
60
40
20
0
10
2
3
4
5
6
7
8
9
100
2
3
4
5
6
7
Particle Diameter (nm)
Total Ambient
Reactor
AMS
SMPS

Figure S6.

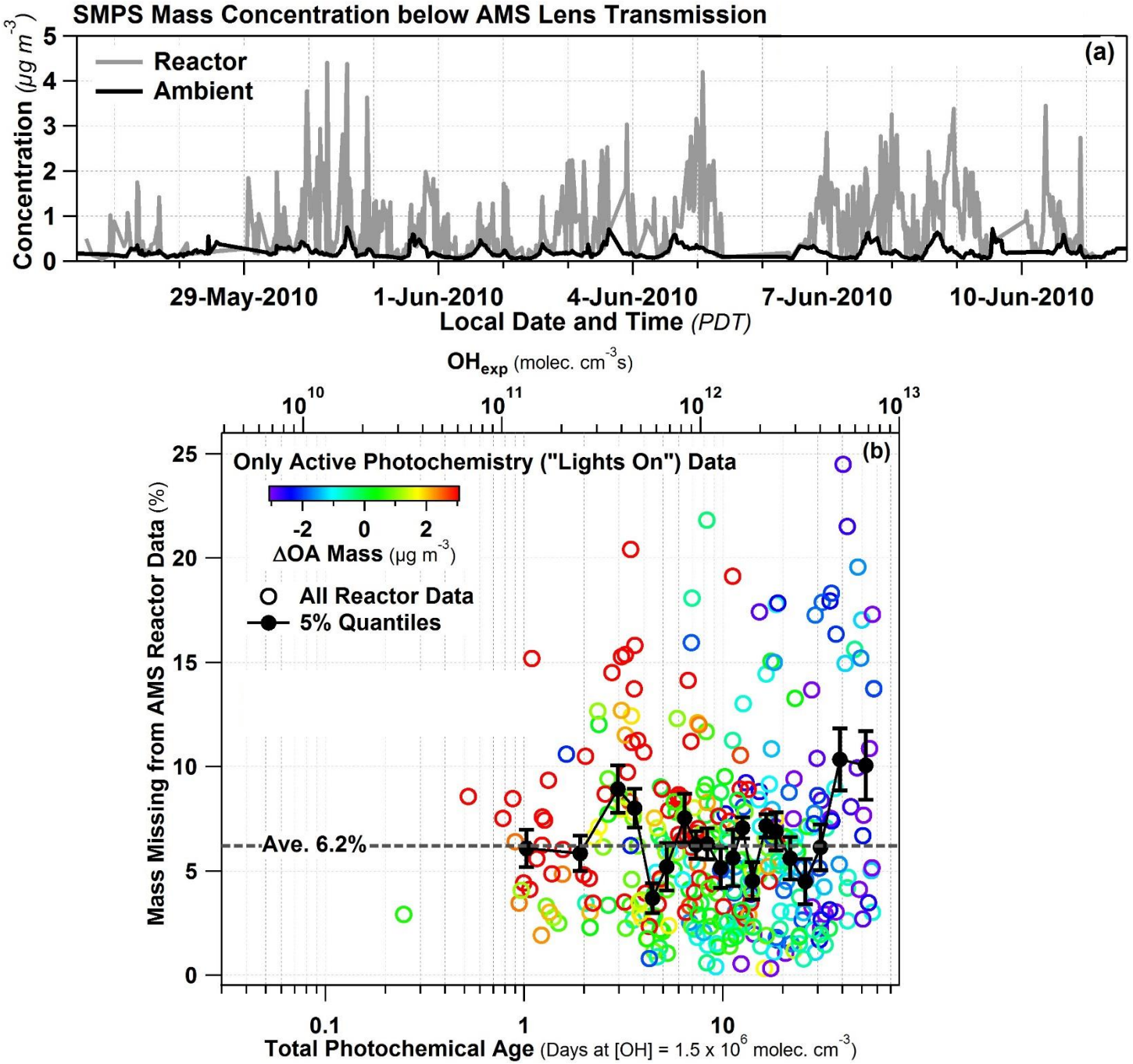
SMPS Mass Concentration below AMS Lens Transmission
Reactor
Ambient
(a)
Concentration (μg m-3)
0
1
2
3
4
5
29-May-2010
1-Jun-2010
4-Jun-2010
7-Jun-2010
10-Jun-2010
Local Date and Time (PDT)
OHexp (molec. cm-3s)
10^10
10^11
10^12
10^13
(b)
Only Active Photochemistry ("Lights On") Data
-2
0
2
ΔOA Mass (μg m-3)
All Reactor Data
5% Quantiles
Ave. 6.2%
Mass Missing from AMS Reactor Data (%)
0
5
10
15
20
25
0.1
1
10
Total Photochemical Age (Days at [OH] = 1.5 x 10^6 molec. cm-3)

Figure S7.

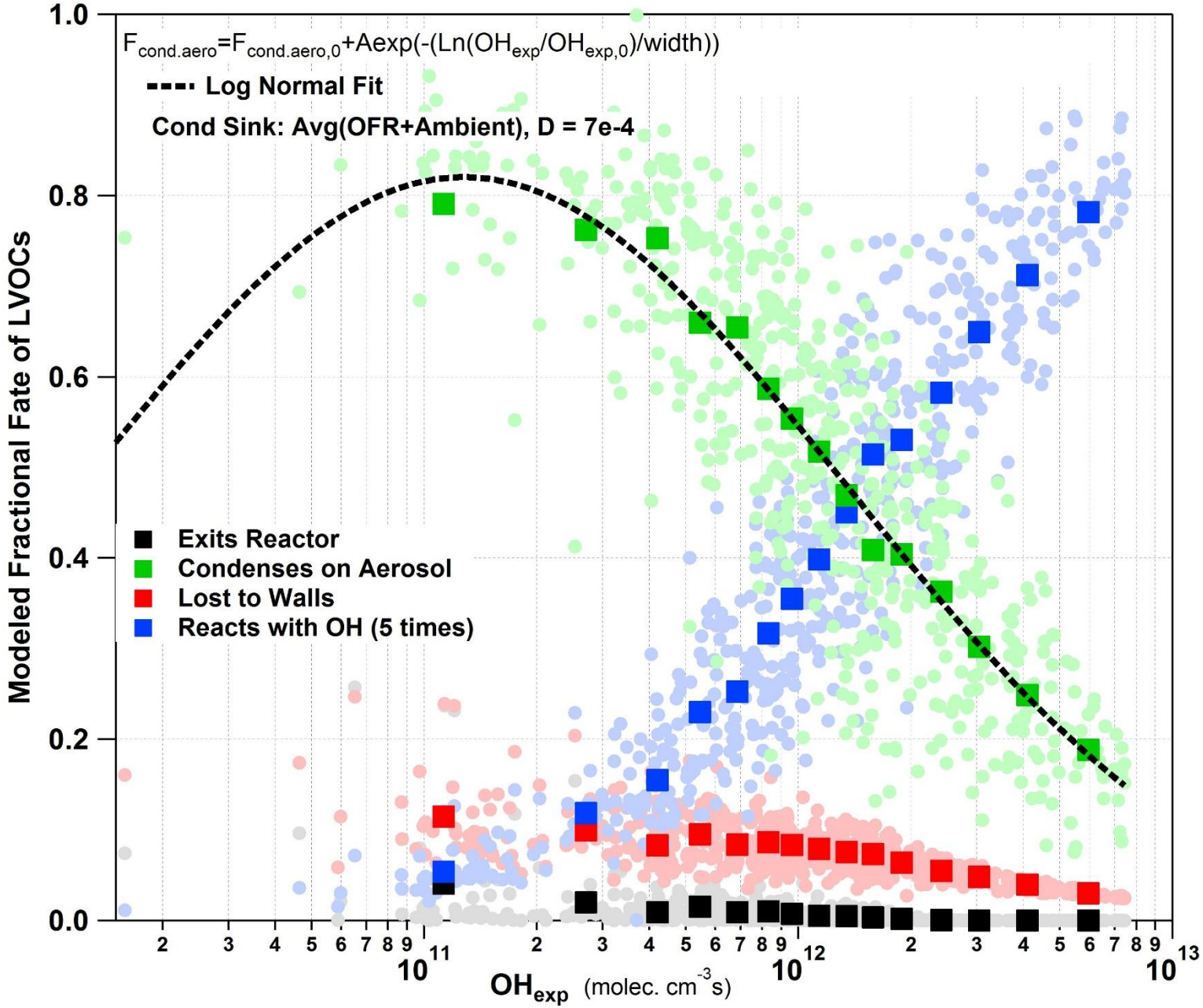
$F_{cond.aero}=F_{cond.aero,0}+Aexp(-(Ln(OH_{exp}/OH_{exp,0})/width))$
Log Normal Fit
Cond Sink: Avg(OFR+Ambient), D = 7e-4
Exits Reactor
Condenses on Aerosol
Lost to Walls
Reacts with OH (5 times)
Modeled Fractional Fate of LVOCs
1.0
0.8
0.6
0.4
0.2
0.0
2 3 4 5 6 7 8 9 10^{11} 2 3 4 5 6 7 8 9 10^{12} 2 3 4 5 6 7 8 9 10^{13}
OH_{exp} (molec. cm^{-3} s)

Figure S8.

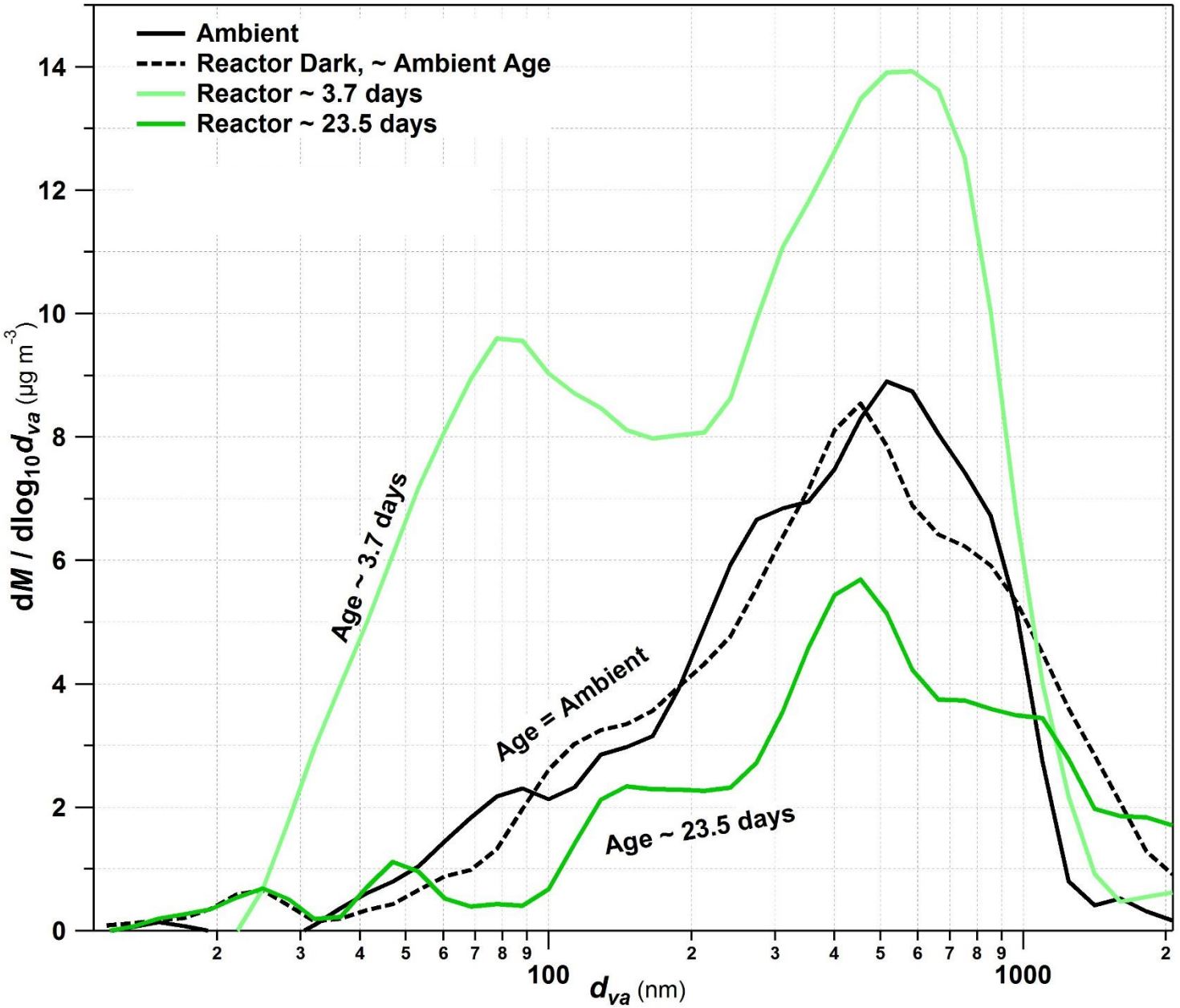
Ambient
Reactor Dark, ~ Ambient Age
Reactor ~ 3.7 days
Reactor ~ 23.5 days
Age ~ 3.7 days
Age = Ambient
Age ~ 23.5 days
dM / dlog10dva (µg m-3)
dva (nm)
0
2
4
6
8
10
12
14
100
1000

Figure S9.

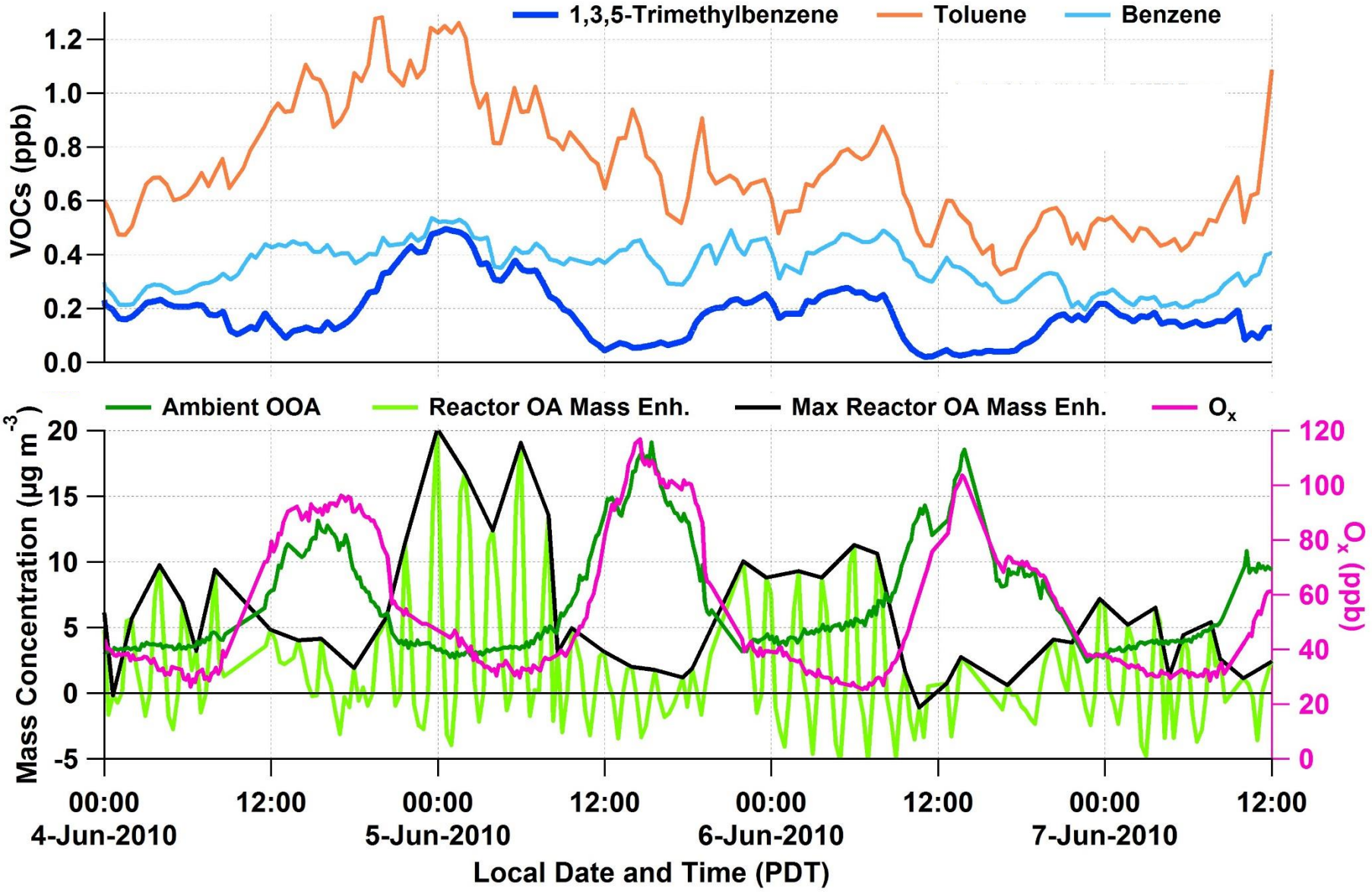
1,3,5-Trimethylbenzene
Toluene
Benzene
VOCs (ppb)
1.2
1.0
0.8
0.6
0.4
0.2
0.0
Ambient OOA
Reactor OA Mass Enh.
Max Reactor OA Mass Enh.
O_x
Mass Concentration (μg m^{-3})
20
15
10
5
0
-5
120
100
80
60
40
20
0
O_x (ppb)
00:00
12:00
00:00
12:00
00:00
12:00
00:00
12:00
4-Jun-2010
5-Jun-2010
6-Jun-2010
7-Jun-2010
Local Date and Time (PDT)

Figure S10.

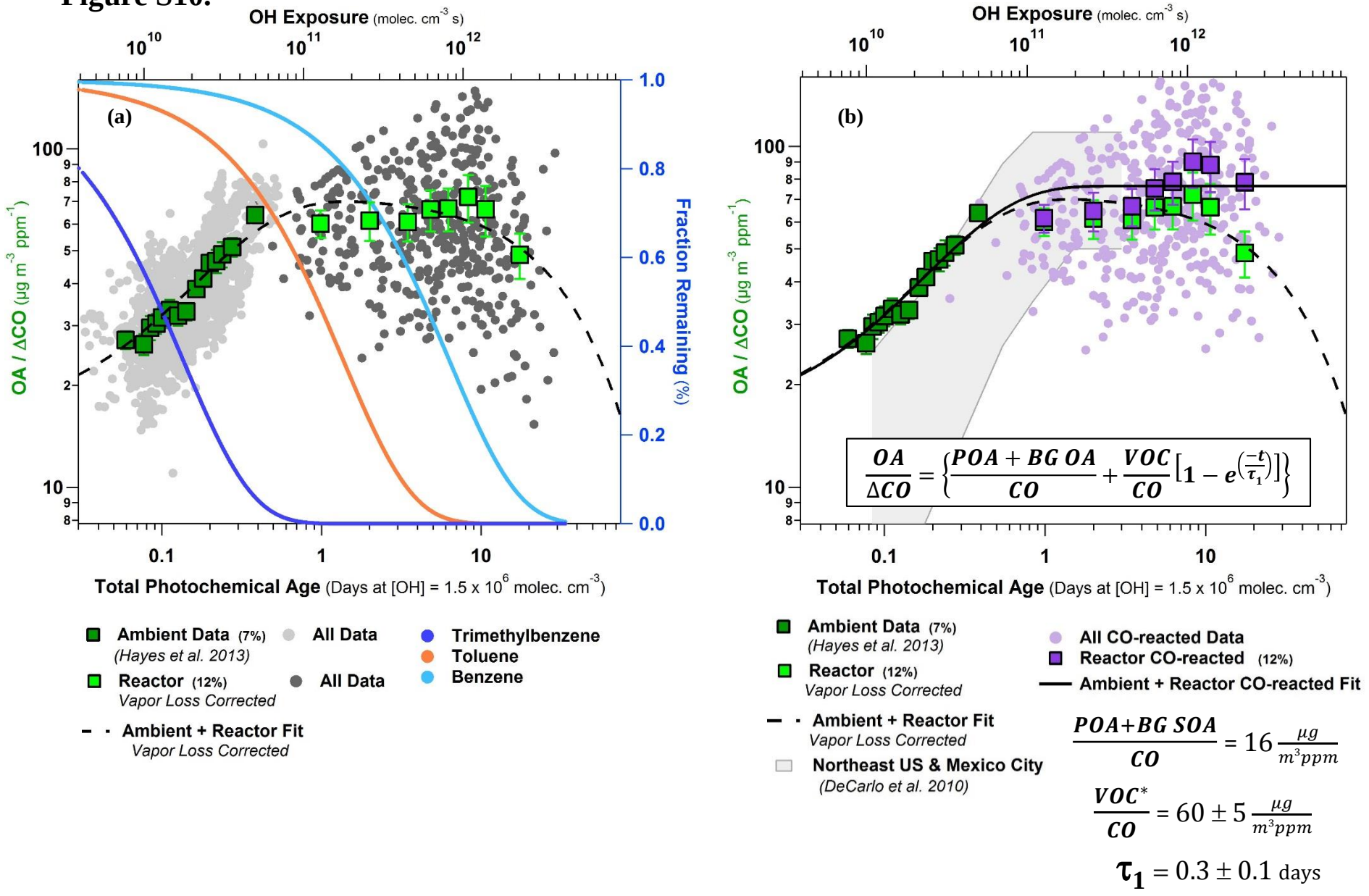
OH Exposure (molec. cm-3 s)
(a)
(b)
OA / ΔCO (μg m-3 ppm-1)
Fraction Remaining (%)
Total Photochemical Age (Days at [OH] = 1.5 x 10^6 molec. cm-3)
Ambient Data (7%)
(Hayes et al. 2013)
Reactor (12%)
Vapor Loss Corrected
Ambient + Reactor Fit
Vapor Loss Corrected
All Data
All Data
Trimethylbenzene
Toluene
Benzene
Ambient Data (7%)
(Hayes et al. 2013)
Reactor (12%)
Vapor Loss Corrected
Ambient + Reactor Fit
Vapor Loss Corrected
Northeast US & Mexico City
(DeCarlo et al. 2010)
All CO-reacted Data
Reactor CO-reacted (12%)
Ambient + Reactor CO-reacted Fit
$\frac{OA}{\Delta CO} = \left\{\frac{POA + BG\ OA}{CO} + \frac{VOC}{CO}\left[1 - e^{\left(\frac{-t}{\tau_1}\right)}\right]\right\}$
$\frac{POA+BG\ SOA}{CO} = 16\ \frac{\mu g}{m^3 ppm}$
$\frac{VOC^*}{CO} = 60 \pm 5\ \frac{\mu g}{m^3 ppm}$
$\tau_1 = 0.3 \pm 0.1$ days

Figure S11.

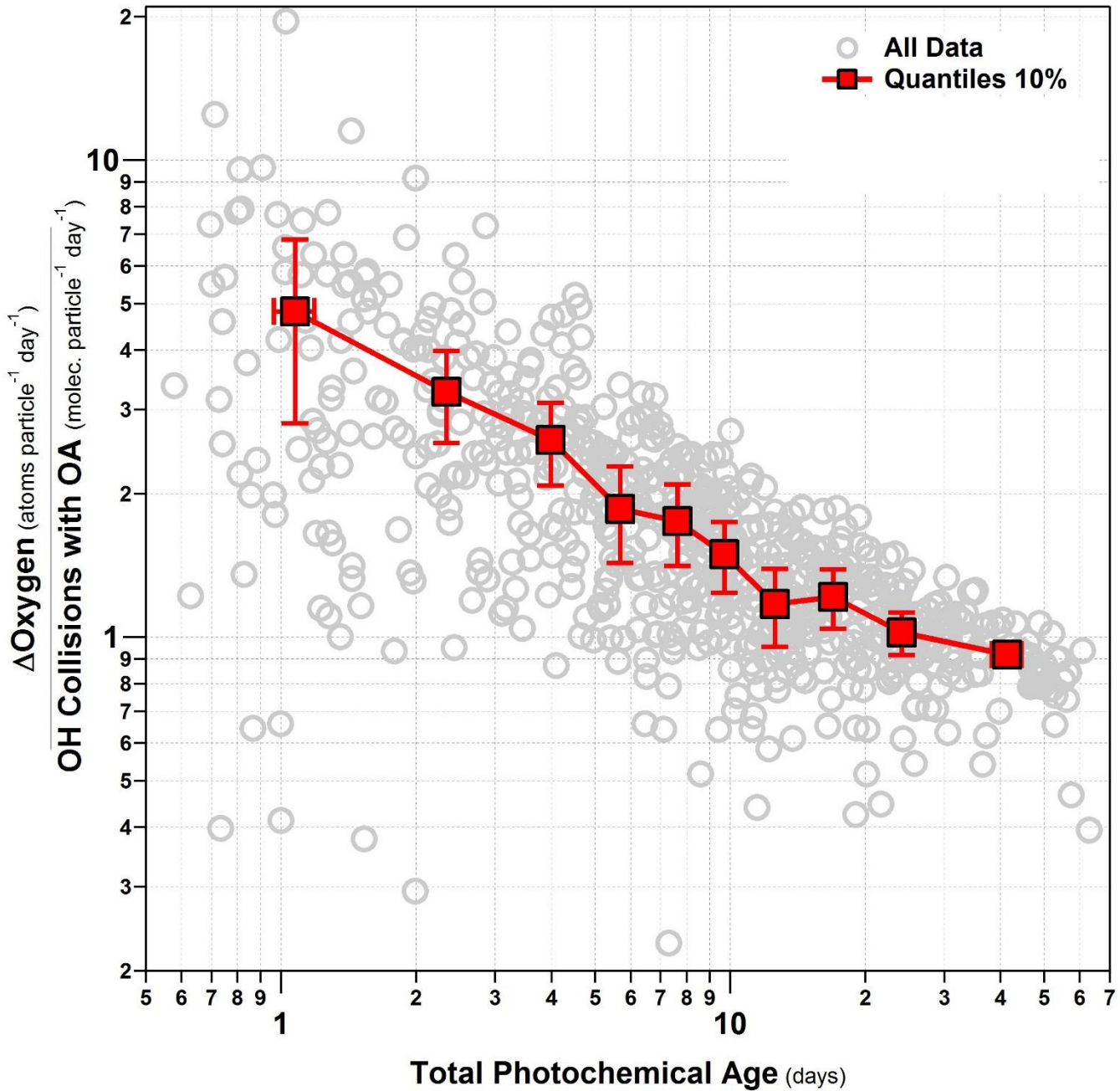
All Data
Quantiles 10%
ΔOxygen (atoms particle-1 day-1)
OH Collisions with OA (molec. particle-1 day-1)
Total Photochemical Age (days)
1
10

Figure S12.

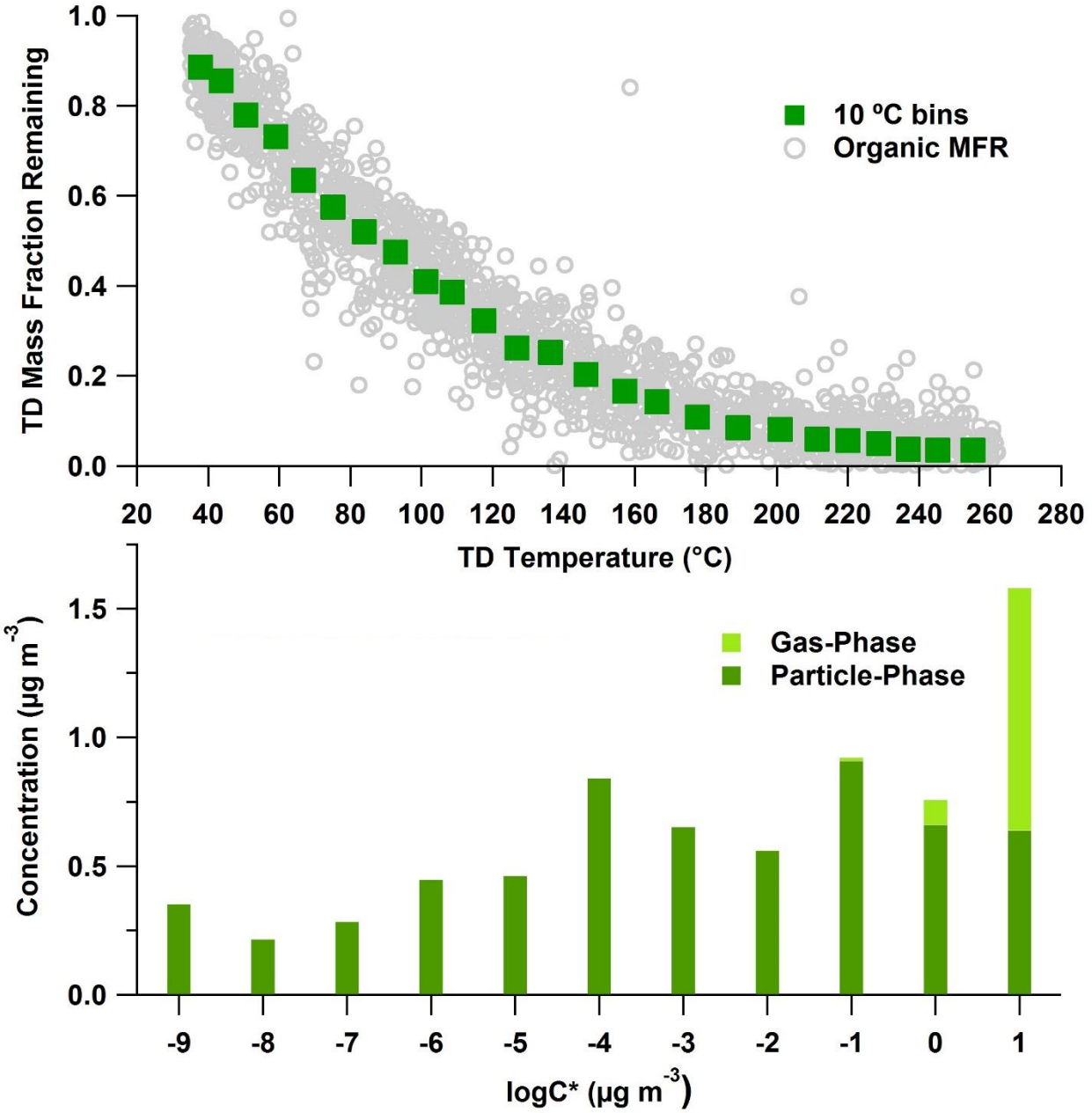
TD Mass Fraction Remaining
1.0
0.8
0.6
0.4
0.2
0.0
10 ºC bins
Organic MFR
20
40
60
80
100
120
140
160
180
200
220
240
260
280
TD Temperature (°C)
Concentration (µg m-3)
1.5
1.0
0.5
0.0
Gas-Phase
Particle-Phase
-9
-8
-7
-6
-5
-4
-3
-2
-1
0
1
logC* (µg m-3)